



HAL
open science

Balanced homodyne detection of Bragg microhologramms in photopolymer for data storage

Frédéric Guattari, Guillaume Maire, Kevin Contreras, Carole Arnaud, Gilles Pauliat, Gérald Roosen, Safi Jradi, Christiane Carre

► **To cite this version:**

Frédéric Guattari, Guillaume Maire, Kevin Contreras, Carole Arnaud, Gilles Pauliat, et al.. Balanced homodyne detection of Bragg microhologramms in photopolymer for data storage. *Optics Express*, 2007, 15 (4), pp.2234-2243. hal-00181708

HAL Id: hal-00181708

<https://hal.science/hal-00181708>

Submitted on 8 Mar 2012

HAL is a multi-disciplinary open access archive for the deposit and dissemination of scientific research documents, whether they are published or not. The documents may come from teaching and research institutions in France or abroad, or from public or private research centers.

L'archive ouverte pluridisciplinaire **HAL**, est destinée au dépôt et à la diffusion de documents scientifiques de niveau recherche, publiés ou non, émanant des établissements d'enseignement et de recherche français ou étrangers, des laboratoires publics ou privés.

Balanced homodyne detection of Bragg microholograms in photopolymer for data storage

Frédéric Guattari¹, Guillaume Maire¹, Kevin Contreras¹, Carole Arnaud¹, Gilles Pauliat¹, Gérald Roosen¹, Safi Jradi², and Christiane Carré³

¹Laboratoire Charles Fabry de l'Institut d'Optique,
Univ Paris-Sud, CNRS, Campus Polytechnique, RD 128 91127 Palaiseau cedex, France.

²Département de Photochimie Générale, UMR CNRS 7525, Maison du Technopôle – Université de Haute Alsace, 34 rue Marc Seguin, 68200 Mulhouse cedex, France.

³Département Optique, UMR CNRS 6082 FOTON, GET-ENST Bretagne,
Technopôle Brest Iroise, CS 83818, 29238 Brest cedex 3, France.

gilles.pauliat@institutoptique.fr

Abstract: Wavelength multiplexed holographic bit oriented memories are serious competitors for high capacity data storage systems. For data recording, two interfering beams are required whereas one of them should be blocked for readout in previously proposed systems. This makes the system complex. To circumvent this difficulty and make the device simpler, we validated an architecture for such memories in which the same two beams are used for recording and reading out. This balanced homodyne scheme is validated by recording holograms in a Lippmann architecture.

© 2007 Optical Society of America

OCIS codes: (210.2860) Holographic and volume memories ; (090.7330) Volume holographic gratings

References and links

1. H. J. Coufal, D. Psaltis, and G. T. Sincerbox, eds., *Holographic Data Storage*, Springer, Series in Optical Sciences (Springer-Verlag, 2000).
2. G. J. Steckman, A. Pu, D. Psaltis, "Storage density of shift-multiplexed holographic memory," *Appl. Opt.* 40, 3387-3394 (2001).
3. S. S. Orlov, W. Phillips, E. Bjornson, Y. Takashima, P. Sundaram, L. Hesselink, R. Okas, D. Kwan, and R. Snyder, "High-transfer-rate high-capacity Holographic disk data-storage system," *Appl. Opt.* 43, 4902-4914 (2004).
4. K. Anderson and K. Curtis, "Polytopic multiplexing," *Opt. Lett.* 29, 1402-1404 (2004).
5. H. Fleisher, P. Pengelly, J. Reynolds, R. Schools, and G. Sincerbox, "An optically accessed memory using the Lippmann process for information storage," *Optical and Electro-Optical Information Processing* (MIT Press, 1965).
6. S. Orlic, S. Ulm, and H.-J. Eichler, "3D bit-oriented optical storage in photopolymers," *J. Opt. A: Pure Appl. Opt.* 3, 72-81(2001).
7. A. Labeyrie, J. P. Huignard, and B. Loiseaux, "Optical data storage in microfibers," *Opt. Lett.* 23, 301-303 (1998).
8. R. R. McLeod, A. J. Daiber, M. E. McDonald, T. L. Robertson, T. Slagle, S. L. Sochava, and L. Hesselink, "Microholographic multilayer optical disk data storage," *Appl. Opt.* 44, 3197-3207 (2005).
9. I. Sh. Steinberg, "Multilayer recording of the microholograms in lithium niobate," in *Photorefractive Effects, Materials and Devices*, Vol. 99 of OSA Trends in Optics and Photonics Series (Optical Society of America, 2005), 610-615.
10. M. Dubois, X. Shi, C. Erben, K.-L. Longley, E.-P. Boden, and B.-L. Lawrence, "Characterization of microholograms recorded in a thermoplastic medium for three-dimensional optical data storage," *Opt. Lett.* 30, 1947-949 (2005).
11. G. Maire, G. Pauliat, and G. Roosen, "Homodyne detection readout for bit-oriented holographic memories," *Opt. Lett.* 31, 175-177 (2006).
12. J.-J. Yang and M.-R. Wang, "White light micrograting multiplexing for high density data storage," *Opt. Lett.* 31, 1304-1306 (2006).
13. R. Jallapuram, I. Naydenova, S. Martin, R. Howard, V. Toal, S. Frohmann, S. Orlic, and H.-J. Eichler, "Acrylamide-based photopolymer for microholographic data storage," *Opt. Mater.* 28, 1329-1333 (2006).

14. A. Murciano, S. Blaya, L. Carretero, R. F. Madrigal, and A. Fimia, "Holographic reflection gratings in photopolymerizable solgel material," *Opt. Lett.* 31, 2317-2319 (2006).
 15. J. M. Bendickson, J. P. Dowling, and M. Scalora, "Analytical expressions for the electromagnetic mode density in finite, one-dimensional, photonic band-gap structures," *Phys. Rev. E* 53, 4107-4121 (1996).
 16. H. Kogelnik, "Coupled wave theory for thick hologram gratings," *Bell Syst. Tech. J.* 48, 2909-2947 (1969).
 17. J. Shamir, "Paradigms for bit-oriented holographic information storage," *Appl. Opt.* 45, 5212-5222 (2006).
-

1. Introduction

Holographic data storage is a serious candidate for the next generation of optical data storage devices with potential capacities exceeding one Terabyte for a 12 cm disk [1]. Most studies have been conducted on page-oriented systems. In these systems the holograms are multiplexed inside the volume of the recording material with, commonly, angular, shift or phase multiplexing [1]. Each stored hologram represents one page of typically 10^6 pixels. Each hologram being recorded and reconstructed at once, these devices are per se massively parallel [2-4].

Bit oriented holographic storage systems are less extensively studied. They nevertheless also present very attractive features such as a better compatibility with conventional surface storage devices [5-14]. Each hologram now represents one bit of data and the recording and readout of these data are commonly achieved bit after bit, although a given amount of parallelism was already demonstrated by simultaneously using several wavelengths [5, 12]. Furthermore, the capacity of this holographic approach favourably compares with the capacity of the page-oriented approach [8]. One-bit holograms are most often recorded by two counter-propagating beams focused inside the medium. This hologram is detected by the Bragg reflection of a reading beam. The wavelength selectivity of reflection holograms allows to record several multiplexed microholograms in the same location, each microhologram being recorded and readout at a given wavelength. In most systems, for recording, only a single beam is sent onto the disk, the counter-propagating beam being provided by a reflection of the reading beam onto a reflective unit placed on the other side of the disk. Most often, this reflective unit is not a part of the disk but lies at a distance beneath the disk [6, 8, 10]. Conversely, in Lippmann structures, this reflective unit is a mirror set in contact with the recording layer. This compact structure increases the stability of the system and reduces the required coherence length of the recording source: recording of such microholograms with a white light source followed by a monochromator has even been successfully demonstrated [5, 12].

Nevertheless, whatever the reflective unit is, for most demonstrated micrograting holographic data storage systems, the reflection on this unit should be prevented during readout in order to detect the diffracted beam only.

Alternatively, we recently proposed a homodyne detection scheme in which the reflection onto the reflective unit is not modified during readout [11]. This homodyne detection is especially attractive for Lippmann data storage approaches in which the mirror is in contact with the sensitive layer and is thus part of the recording structure (optical disk). Therefore, during data readout, the beam diffracted by the recorded hologram interferes with the beam reflected onto the reflective unit. During the homodyne readout, the hologram modifies the interference state: it may increase or decrease the detected signal or just modify the phase of the optical signal according to the relative phase between the two interfering beams. It should be noted that, besides its simplicity, homodyne detection also increases the amplitude of the detected signal compared to the conventional intensity detection of the diffracted signal. The cost to pay for these advantages is the important DC component of the signal that corresponds to the signal reflected onto the reflective unit. In case of low diffraction efficiencies, fluctuations of this DC component (for instance due to power fluctuations of the laser) could mask the signal variations originating from the weak beam diffracted by the hologram.

We previously validated this homodyne detection in a scheme where the mirror was not glued onto the sensitive layer (a photorefractive crystal in this case) [11]. The small air gap between the 50% mirror and this layer allowed us to make the mirror oscillate at frequency ω with an amplitude much smaller than the optical wavelength. With a lock-in amplifier set at

frequency ω , we were able to extract the beating signal between the two interfering beams, which makes the detection insensitive to the strong DC component.

Although this first demonstration validated the principle of the homodyne detection, it is not transposable to a realistic disk system in which the mirror would be in contact with the sensitive layer. In this communication we investigate a new scheme for homodyne detection that is compatible with Lippmann data disks.

2. Principle of the balanced homodyne detection

The principle of the detection scheme we investigate in this communication is illustrated in Fig. 1. The Lippmann mirror, whose reflectivity should be below 100%, and is typically about 50% in our experiments, is set in contact with the sensitive layer. The recording beam is focused onto this mirror through the sensitive layer so that it interferes with its reflection on the mirror. These interferences record the Bragg grating. Several gratings can overlap in the same location by tuning the wavelength of the optical source. For reading out, we propose to probe the grating by the beam used for recording, without modifying the set-up. Two signals, S_R and S_T , respectively corresponding to the reflected beam and the transmitted beam, are detected. They can be expressed as:

$$\begin{cases} S_R = \alpha R I \\ S_T = \beta T I \end{cases} \quad (1)$$

with I the reading intensity, α and β proportionality constants taking into account the gain of the photodiodes, R and T the reflectivity and transmission coefficients of the structure "hologram-mirror".

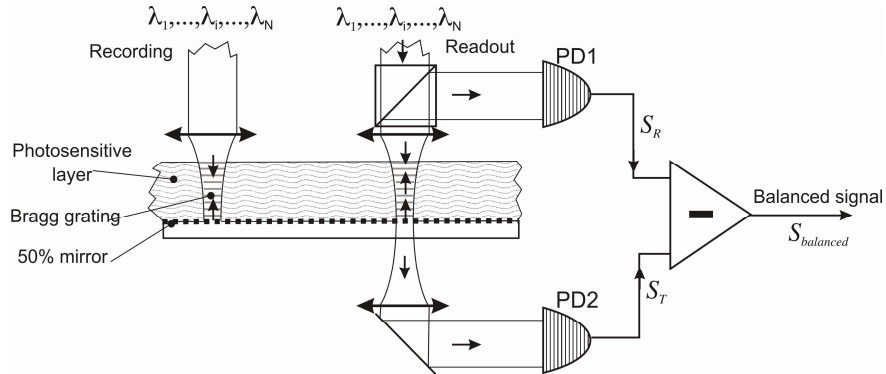


Fig. 1. Principle of balanced homodyne detection. PD1 and PD2 are two photodiodes providing the two homodyne signals, which are subtracted to get the balanced signal.

In the presence of hologram, R and T differ from the reflectivity R_0 and transmission T_0 of the mirror alone. For a lossless system we get:

$$R = R_0 + \Delta R \quad \text{and} \quad T = T_0 - \Delta R \quad (2)$$

with ΔR being the variation of reflectivity induced by the hologram. Although not mentioned, ΔR is a function of the readout wavelength.

The signal of interest, proportional to ΔR , is easily extracted by performing a balanced detection between the two normalized signals:

$$S_{balanced} = \alpha R_0 S_T - \beta T_0 S_R = -\beta \alpha I \Delta R \quad (3)$$

The two normalization coefficients can be experimentally determined by adjusting the gains of the two photodiodes in order to nullify $S_{balanced}$ in the case when no hologram is present.

3. Experimental set-up

The experimental set-up is depicted in Fig. 2. It is made of two identical optical heads. Each head is fed by a single-mode polarization-maintaining optical fibre. The beams from the fibres are first collimated by aspheric lenses L_1 (focal length 4 mm) and then focused again by aspheric lenses L_2 (focal length 11 mm) onto the Lippmann mirror. The beam waist on the mirror is about $5 \mu\text{m}$. We do not use the fibres to collect the beams transmitted and reflected by the Lippmann sample. Indeed, the structure of these beams differs from the nearly-gaussian shape of the mode of the fibres: light coupling of these beams inside the fibres is quite inefficient. Therefore inside each couple of lenses L_1-L_2 is inserted a beam splitter to respectively extract the reflected and transmitted signals. The Lippmann sample is held on a $x-y$ piezo-translation stage whose excursion range is $100 \times 100 \mu\text{m}^2$. This piezo-translation stage is itself mounted on a rotation stage whose rotation axis is along the y axis and lies in the plane of the Lippmann mirror. This rotational motion is used to probe the angular dependence of the hologram diffraction efficiency.

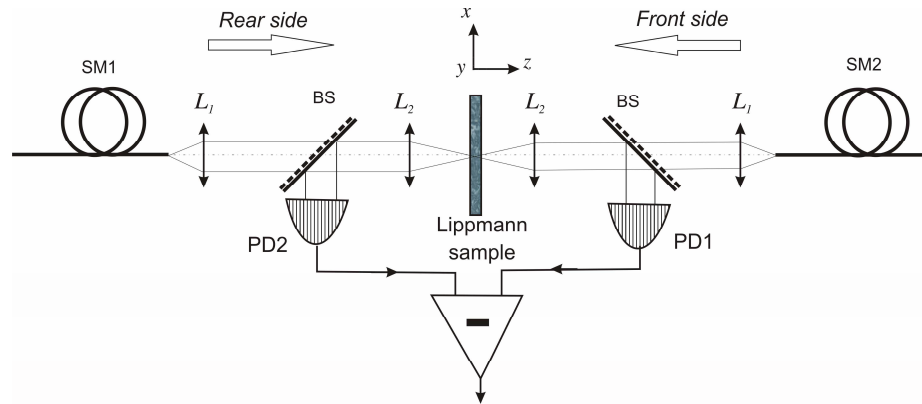


Fig. 2. Scheme of the experimental set-up used to validate the balanced homodyne detection. BS are beam splitters, PD1 and PD2 photodiodes.

The Lippmann sample is shown in Fig. 3. The hologram is recorded by photopolymerization. This photopolymerizable layer is a solvent-free mixture of a photoinitiator (Eosin Y), of an amine as a cosensitizer (N-methyl diethanolamine) and of a liquid monomer base (pentaerythritol triacrylate). It is embedded between two glass plates, a substrate and a superstrate. Its thickness, $160 \pm 5 \mu\text{m}$, is defined by metallic spacers. The external faces of the glass plates are anti-reflection coated to minimize the parasitic reflections that could interfere with the homodyne signal. On its facet in contact with the sensitive layer, the substrate glass plate received a coating to act as a mirror. Its intensity reflectivity is about 60%. For the glass material, we selected BK7 as its refractive index is close to the refractive index of the formulation. This refractive index matching minimizes the Fresnel reflections at the interface polymer-superstrate. The thickness of each glass plate is 1.6 mm. This thickness was selected large enough so that the beams reflected by the residual reflection onto the anti-reflection coatings do not properly overlap with the beams reflected and transmitted by this mirror. These reflections do not corrupt the homodyne signal.

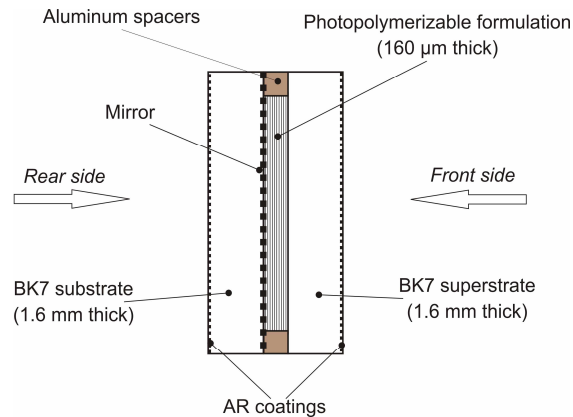


Fig. 3. Structure of the Lippmann structure. The pre- and post-exposures and the hologram readout are achieved by sending the beam from the rear-side, while the hologram recording is made from the front-side.

For recording and probing the holograms, we used two Fabry-Perot diodes from Nichia. The beams from these two diodes can be injected inside the two optical fibres to feed the recording set-up either from the rear side or the front side (see Figs. 2 and 3). One diode emits around 473 nm and the other one around 475 nm. Their wavelengths can be slightly tuned with the temperature, but we did not use this possibility as this tuning is not continuous and also as it considerably changes the spectral width of the emitted beam. For the experiments reported below, the diodes usually oscillate on a few longitudinal modes with a spectral width of about 0.5 nm. The coherence length is thus larger than the photosensitive layer thickness, so that the holograms are recorded with a maximum modulation ratio over this whole 160 μm thickness.

3.1 Recording of reflection holograms with plane-waves

As we will show in a next section, the sign of the modifications of the R and T coefficients of the Lippmann structure [Eq. (1) and Eq. (2)] resulting from the hologram recording with focused beams differ from those obtained with planes waves. To better understand these latter results, we first tested the recording of reflection holograms using “plane-waves” and probed these holograms at various angles to simulate the plane wave components of a focused beam. This first approach also allowed us to determine the best exposition parameters (exposure intensity and time).

In order to record holograms with “plane-waves”, we removed lenses L_2 (see Fig. 2) from the optical set-up. Without these lenses, the beams launched from the optical fibres are collimated by lenses L_1 . The waist of these beams onto the Lippmann structure is about $\omega \approx 300 \mu\text{m}$ so that their associated Rayleigh length is about 90 cm (taking into account the refractive index of the photopolymer). These beams can thus be considered as crude approximations of plane waves through the 160 μm of the sensitive layer.

The photopolymerizable formulation we are using suffers from a very large shrinkage that may fully perturb the hologram recording and reading out (ca 10% for photocuring experiments with these acrylates). Usually, optical shrinkage originates from a variation of the material thickness and from a change of the polymer refractive index following the photopolymerization. In our experiment, because of the presence of the thick glass plates, exposing the material over a small area does not change the thickness of the active layer. It just changes its refractive index.

In an independent experiment we previously determined that this shrinkage corresponds to a refractive index change of about $\Delta n_{\text{max}} \approx 0.012$. The consequence of this refractive index change is, at least, two-fold:

- 1) it modifies the optical wavelength during recording and thus blurs the fringes;
- 2) it creates a short focal length refractive index lens that alters the beam propagation.

These two effects prevent the efficient recording and readout of microholograms. The first point could be alleviated by using an exposure time much shorter than the complete photopolymerization duration, which is typically of a few seconds. Nevertheless, this refractive index change would still change the Bragg wavelength, modification that cannot be compensated in our set-up.

In order to circumvent these two problems, we used a strong uniform pre-exposition to consume most of the refractive index dynamic range. This pre-exposition is conducted by sending a beam from the rear fibre to the rear-side of the Lippmann structure in order to avoid recording gratings inside the photopolymer (see Fig. 3). The energy incident onto the photopolymer during the pre-exposition is about 0.2 J/cm^2 using an optical intensity of about 3 mW/cm^2 . From our previous measurements on the photopolymer, we estimate that this pre-exposition consumes most of the available refractive index change. Consequently, we evaluate that the maximum index change that could appear during hologram recording is smaller than $\Delta n_{\text{expo}} \approx 0.1\%$ corresponding to a shift of the Bragg wavelength smaller than $\Delta\lambda = -\lambda \Delta n/n \approx 0.3 \text{ nm}$. Such a shift is smaller than the expected Bragg selectivity.

The pre-exposition beam is then blocked and we proceeded with the recording of the grating by sending a beam through the front-side of the Lippmann structure and at normal incidence. We wrote this grating with a beam of $\omega \approx 300 \mu\text{m}$ radius during 30 s with an optical intensity around 10 mW/cm^2 at 473 nm .

Detection of the grating can be achieved either by analyzing the reflection or the transmission of the structure. Similarly, this reflection (or this transmission) can be equivalently probed by the rear-side or the front-side of the structure. It is indeed known that the intensity reflectivities of such periodic structures are the same from both the forward and backward directions [15]. For the sake of experimental convenience, we probed this recorded grating by sending the beam from the same laser diode on the rear-side and by detecting the transmitted signal. By doing so, we avoided recording of any further gratings during this readout.

Because of the fixed wavelength of our laser source, we tested this grating by rotating the sample around the y axis and by detecting the transmitted beam versus this rotation angle. The measured signal detected by photodiode PD1 is shown in Fig. 4 versus the angle of refraction. This signal presents a fast oscillating feature that originates from the Fabry-Perot interferences between the homodyne signal and the residual reflection onto the anti-reflection coating of the superstrate. The mean of these oscillations represents the desired homodyne signal versus the angle.

In order to analyze this signal, we modeled the light transmission through the Lippmann structure, using coupled wave equations [16]. For this modeling, we assumed a zero optical shrinkage (as a result of the very strong pre-irradiation) and a positive value of the refractive index modulation, i.e. that the bright fringes of the interference pattern correspond to an increase of the refractive index above its mean value. The only fitting parameter we used for this modeling is this amplitude of the refractive index modulation of the grating. We fitted it to the value $\delta n \approx 1.1 \cdot 10^{-4}$.

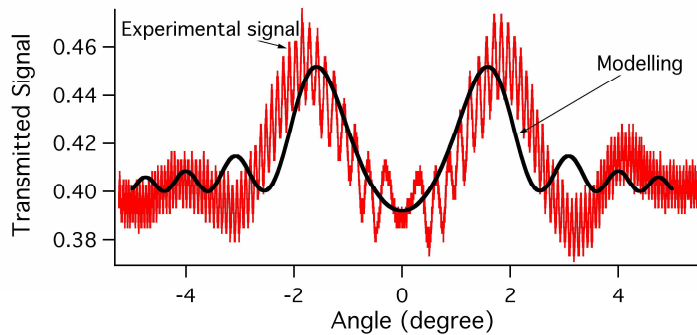


Fig. 4. Experimental (oscillating line) signal transmitted by the hologram-mirror structure, versus the refraction angle. This curve is obtained by rotation of the Lippmann sample along the y axis (see Fig. 2). The black solid line is the theoretical fit (see text).

It is worth noting that this value for δn corresponds to a modification of the transmission of about 6%, while it would have corresponded to a diffraction efficiency of about only 1% if this homodyne detection were not used. These values highlight the signal gain obtained with homodyne detections [11].

Except for the fast oscillating part corresponding to the parasitic Fabry-Perot as explained above, the agreements between the experiment and the modeling are satisfactory. The main features of these curves can be analyzed as follows.

- For large incident angle, the diffraction efficiency of the Bragg grating vanishes because of Bragg selectivity, and the transmission of the sample is equal to the transmission of the mirror alone, about 40%.
- At normal incidence, the transmission of the structure is also close to the mirror transmission, and consequently, the reflectivity of the structure is close to the mirror reflectivity. This originates from the $\pi/2$ phase difference between the diffracted beam and the reflected beam. This $\pi/2$ phase shift comes from diffraction over a refractive index grating which is in-phase with the recording interference pattern. This feature confirms that our pre-exposure schedule makes shrinkage negligible and that the Bragg wavelength is equal to the recording wavelength.
- When the angle starts to depart from 0° , we observe an increase of the signal (corresponding to a decrease of the reflectivity). This increase originates from the additional phase shift resulting from the off-Bragg diffraction process [15]. This is an increase of the transmitted signal, which is coherent with the positive sign of the refractive index modulation δn .
- The Bragg angular selectivity half-width is slightly larger than the theoretical one, which indicates that the grating is slightly non-uniform through the sample thickness.

All these features confirm our correct mastering of the recording medium. Nevertheless, the Fabry-Perot effect is clearly detrimental to the correct operation of the signal detection. The straightforward way to avoid it is to use focused beams so that the wavefront of the homodyne signal beams (reflected on the mirror and diffracted by the hologram) strongly differs from this parasitic reflected beam. This experiment is the subject of the next section.

3.2 Balanced homodyne detection of Lippmann microgratings

In order to get rid of the oscillation of the homodyne signal originating from the spurious reflections, we have been using focused beams. Therefore, lenses L_2 were inserted in the two optical heads. The beam waist on the Lippmann mirror is now about $\omega \approx 5 \mu\text{m}$. This value

corresponds to a Rayleigh length of about $249\ \mu\text{m}$. This value is larger than the sensitive layer, so that relatively uniform holograms can be recorded over its $160\ \mu\text{m}$ thickness. Nevertheless, it remains much smaller than the superstrate thickness so that the radius of curvature of the beam reflected onto the mirror and the one reflected onto the anti-reflection facet of the superstrate are quite different. This difference of radii of curvature minimizes the detrimental Fabry-Perot effect observed above with plane-waves.

In order to minimize the optical shrinkage, we pre-exposed the sensitive layer as done previously, i.e. from the rear-side of the Lippmann structure. By scanning the optical spot with the piezoelectric translation stage, we uniformly exposed an area of $100\times 100\ \mu\text{m}^2$ during 145 s and with an optical power of $0.6\ \mu\text{W}$. Then, from the front-side, we recorded a hologram at normal incidence during 0.5s with an optical power of $320\ \mu\text{W}$ and with the laser diode emitting at the wavelength of 475 nm. This large energy totally consumes the remaining refractive index change. During this recording, the piezo-translation stage is fixed. Subsequently, in order to definitively stabilize the hologram (i.e. to reach full completion of the chemical reaction), we proceeded with a post-irradiation from the rear-side similar to the pre-exposition.

The hologram is then readout from the rear-side with the diode used for recording and set at 475 nm. The transmitted and reflected signals are detected by photodiodes PD1 and PD2 while scanning the spot over an area of $100\times 100\ \mu\text{m}^2$. The scan of the homodyne transmitted and reflected signals are shown in the left of Figs. 5(a) and 5(b) respectively. Figure 5(c) left represents the balanced signal. To plot these figures, we normalized the signals to unity in the absence of the hologram.

For the sake of comparison, we also performed the same readout procedure by using the second laser diode set at a wavelength of 473 nm. The corresponding measurements are plotted in the right of Figs. 5(a), 5(b), and 5(c), which represent respectively the homodyne transmitted signal, the homodyne reflected signal and the balanced signal. The small bumps in the corners of the scanning area correspond to the limit of the pre-exposition area and thus to non-uniform exposition zones. They should thus not be considered.

In order to test the reproducibility of our measurements, we repeated several times and at different locations such hologram recordings and readouts. All the obtained results are very similar: using the same wavelength for the readout as the one used for recording, the presence of the hologram always increases the transmitted beam and decreases the reflected beam.

The width of the detected signal results from a convolution of the hologram width with the beam width. In the experiment reported in Fig. 5, we estimate the hologram radius to be around $25\ \mu\text{m}$. This width is larger than the beam waist and results from the very large energy used to expose the hologram. With lower energies we obtained smaller widths, down to a radius of about $5\ \mu\text{m}$, but these holograms are more difficult to control and to characterize with our photopolymer.

One clearly sees the presence of the hologram in the left of Fig. 5 whereas the signal is much lower when reading at the smaller wavelength in right of Fig. 5. We also performed other experiments in which the holograms were written at the smaller wavelength of 473 nm and readout at both wavelengths. In this last case, we also clearly observed the presence of the hologram at 473 nm, while at 475 nm we observed weaker signals which are opposite in sign to the signals detected at 473 nm (that is a small increase of the reflectivity and small decrease of the transmission). By temperature tuning the diodes, we were also able to probe the gratings at some other wavelengths. From these experiments we estimate that the Bragg wavelength selectivity of our homodyne detection for those holograms is about 2 nm. Although this estimation is very crude, it is much larger than the Bragg selectivity half-width, $\Delta\lambda = \lambda^2 / (2ne) \approx 0.5\ \text{nm}$, computed from the successful plane-wave approach used to analyse the results presented in the previous section. This result is not surprising. It is indeed known that the Bragg selectivity half-width of microgratings is much larger than the Bragg selectivity of plane-wave gratings [17]. This increase of the Bragg selectivity half-width is also visible from the experiments reported in Ref. [14].

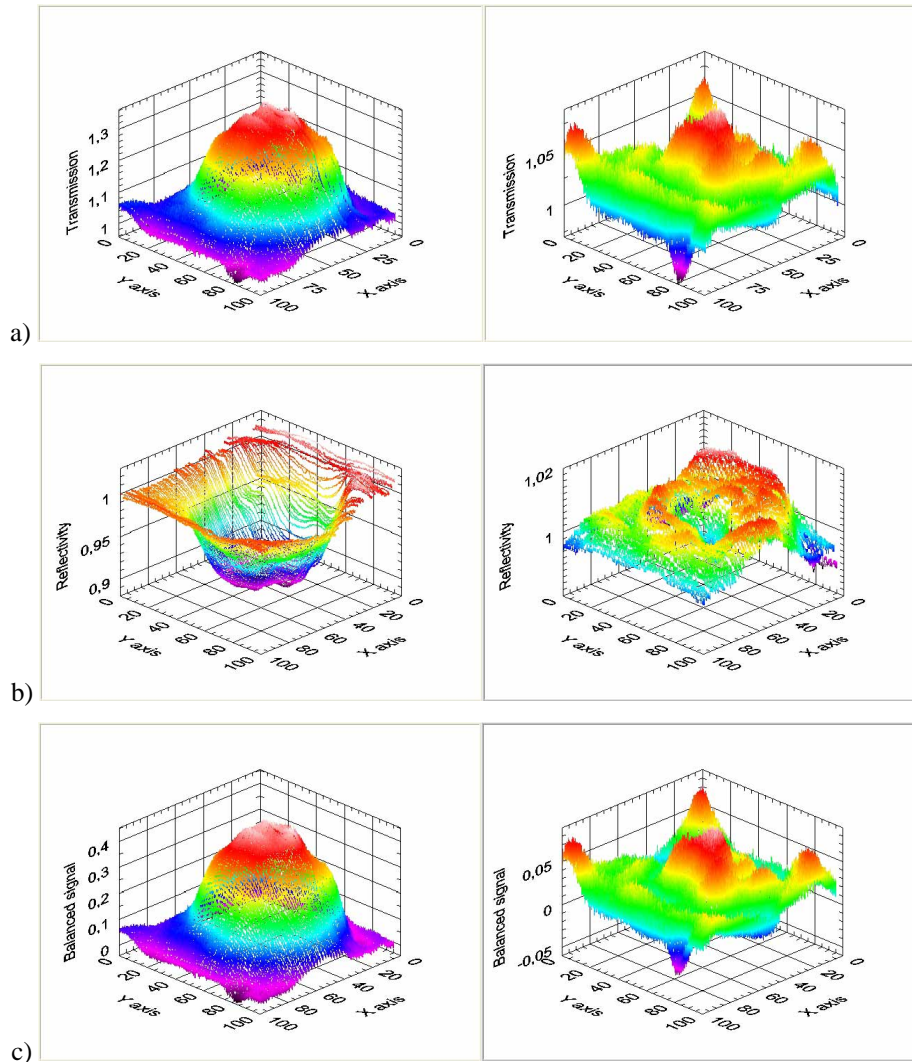


Fig. 5. Signals detected by scanning the piezoelectric translation stage along the x and y axes: a) homodyne transmitted signal; b) homodyne reflected signal; c) balanced signal. The left images are obtained with the diode at the wavelength of 475 nm used for hologram recording, and the right images with the diode at the wavelength of 473 nm, i.e. 2 nm below the wavelength used for recording.

This increased Bragg selectivity half-width and also the sign of the homodyne signal can be interpreted as follows. The recorded hologram is wider than the probe beam. On the scale of the probe beam, and in a first crude approximation, it can be considered as infinite. This probe beam is a Gaussian focused beam with a waist of about $\omega \approx 5 \mu\text{m}$, which corresponds to a half-angular spread of: $\theta_{1/e} = \lambda / (n\pi \omega) \approx 20 \text{ mrad} \approx 1.2^\circ$. This probe beam thus contains a full spread of plane-waves. Referring to Fig. 4, one sees that each of them probes the grating with a different refraction angle and thus experiences a different transmission. For the plane wave components with a refraction angle very close to zero, the transmission is not modified by the hologram, however, for plane-waves with a larger angle, we observed a slight increase of the transmission. In our set-up we integrate all these plane-wave components onto the photodiodes so that, overall, we observe an increase of the transmitted signal.

Nevertheless, the correct operation of the homodyne detection only requires that the reflected and transmitted homodyne signals varies with opposite signs in presence of a hologram; no matter which one increases. Indeed, Fig. 5 illustrates the perfect behaviour of this proposed balanced detection scheme. The two homodyne signals [Figs. 5(a) and 5(b) left] vary in opposite directions so that the balanced signal computed using Eq. (3) allows to double the signal corresponding to the presence of the grating while cancelling out the DC components due to the reflectivity R_0 and transmission T_0 of the mirror alone. By reading out at a wavelength 2 nm larger than the Bragg wavelength, one clearly sees in the right of Fig. 5 that the balanced signal vanishes.

4. Conclusion

We have validated a balanced detection scheme for microholograms. This scheme is particularly convenient with the Lippmann architecture as the Lippmann mirror does not need to be removed, nor masked, during the data readout. Furthermore, this homodyne detection considerably enhances the amplitude of the detected signal. This point is of first importance for high capacity holographic data storage in which multiplexing a large number of holograms considerably decreases the retrieved signals. Moreover, because it efficiently removes the DC component of the unbalanced homodyne signal, this balanced detection is more robust to the power fluctuations of the optical source than a simple unbalanced detection. This is all the more important since the power emitted by tunable sources may vary with the wavelength.

Acknowledgment

This work was supported by grants from Région Ile-de-France.